Short Article

Developmental Cell

Formin-like 2 Promotes β1-Integrin Trafficking and Invasive Motility Downstream of PKCα

Highlights

- FMNL2 is phosphorylated at S1072 and activated by PKCα
- FMNL2 undergoes rapid relocation upon PKCα activation
- S1072 of FMNL2 mediates binding of the formin to the α-integrin GFFKR core sequence
- FMNL2 promotes integrin internalization and cell invasion downstream of PKCα

Authors

Ying Wang, Antti Arjonen, Jeroen Pouwels, ..., Oliver T. Fackler, Johanna Ivaska, Robert Grosse

Correspondence

robert.grosse@staff.uni-marburg.de

In Brief

Actin dynamics and integrin turnover are essential for tumor cell migration. Wang et al. show that interaction of the formin-like 2 (FMNL2) actin assembly factor with integrins controls the internalization of these adhesion receptors to promote cancer cell invasion. This mechanism requires the phosphorylation and activation of FMNL2 by PKCα.

Wang et al., 2015, Developmental Cell *34*, 475–483
August 24, 2015 ©2015 Elsevier Inc.
http://dx.doi.org/10.1016/j.devcel.2015.06.015

CellPress

Developmental Cell
Short Article

Formin-like 2 Promotes β1-Integrin Trafficking and Invasive Motility Downstream of PKCα

Ying Wang,[1] Antti Arjonen,[2] Jeroen Pouwels,[2] Haisen Ta,[3] Patrick Pausch,[4] Gert Bange,[4] Ulrike Engel,[5] Xiaoyu Pan,[6] Oliver T. Fackler,[6] Johanna Ivaska,[2,7] and Robert Grosse[1,*]
[1]Institute of Pharmacology, University of Marburg, 35043 Marburg, Germany
[2]Turku Centre for Biotechnology, University of Turku, 20520 Turku, Finland
[3]Department of NanoBiophotonics, Max Planck Institute for Biophysical Chemistry, 37077 Göttingen, Germany
[4]LOEWE Center for Synthetic Microbiology (SYNMIKRO) and Department of Chemistry, University of Marburg, 35043 Marburg, Germany
[5]Nikon Imaging Center and COS, University of Heidelberg, 69120 Heidelberg, Germany
[6]Department of Infectious Diseases, Integrative Virology, University Hospital Heidelberg, 69120 Heidelberg, Germany
[7]Department of Biochemistry and Food Chemistry, University of Turku, 20520 Turku, Finland
*Correspondence: robert.grosse@staff.uni-marburg.de
http://dx.doi.org/10.1016/j.devcel.2015.06.015

SUMMARY

Regulated turnover of integrin receptors is essential for cell adhesion and migration. Pathways selectively regulating β1-integrin recycling are implicated in cancer invasion and metastasis, yet proteins required for the internalization of this pro-invasive integrin remain to be identified. Here, we uncover formin-like 2 (FMNL2) as a critical regulator of β1-integrin internalization downstream of protein kinase C (PKC). PKCα associates with and phosphorylates FMNL2 at S1072 within its Diaphanous autoregulatory region, leading to the release of formin autoinhibition. Phosphorylation of FMNL2 triggers its rapid relocation and promotes its interaction with the cytoplasmic tails of the α-integrin subunits for β1-integrin endocytosis. FMNL2 drives β1-integrin internalization and invasive motility in a phosphorylation-dependent manner, while a FMNL2 mutant defective in actin assembly interferes with β1-integrin endocytosis and cancer cell invasion. Our data establish a role for FMNL2 in the regulation of β1-integrin and provide a mechanistic understanding of the function of FMNL2 in cancer invasiveness.

INTRODUCTION

Spatiotemporal control of receptor internalization is essential in regulating cell surface receptor turnover and ligand interaction for downstream signaling. This is in particular true for integrin adhesion receptors that undergo constant endocytic and exocytic traffic necessary for cell motility and cytokinesis (Caswell and Norman, 2008; De Franceschi et al., 2015) and deregulation in the dynamic recycling of integrins, such as the α5β1 heterodimer, facilitates cancer invasion and metastasis (Caswell et al., 2008; Jacquemet et al., 2013; Muller et al., 2009).

Actin filament assembly can generate mechanical forces to induce membrane deformation (Kaksonen et al., 2006) and to facilitate vesicle trafficking, providing a platform to affect receptor turnover (Zech et al., 2012). It is not clear whether formins being the largest group of actin nucleation and assembly factors play a role in integrin traffic and function. Formins are defined by their formin homology 2 (FH2) domain (Baarlink et al., 2010; Breitsprecher and Goode, 2013). Most formins function as effectors for Rho-GTPases and are regulated by the intramolecular binding between the Diaphanous inhibitory (DID) and autoregulatory (DAD) domains (Faix and Grosse, 2006). Formins are involved in a variety of actin-dependent membrane processes ranging from filopodia formation (Schirenbeck et al., 2005), cell spreading (Iskratsch et al., 2013), and non-apoptotic blebbing (Kitzing et al., 2007; Stastna et al., 2012) to engulfment and phagocytosis (Brandt et al., 2007; Seth et al., 2006). FMNL2 is unique among formins as it is upregulated in several metastatic cancers and is involved in cancer cell behavior and progression (Li et al., 2010; Liang et al., 2013; Zhu et al., 2011, 2008), but the underlying molecular mechanisms are not well understood.

Members of the protein kinase C family have been implicated in integrin traffic. PKCα mediates β1-integrin internalization and PKCε regulates its recycling back to the plasma membrane (Ivaska et al., 2002; Ng et al., 1999). In fibroblasts, attenuation of α5β1-integrin-mediated adhesion upon engagement of syndecan-4 involves PKC activity (Bass et al., 2011). However, the mechanistic details and downstream targets of PKC in integrin traffic remain unknown.

Here we provide evidences for an involvement of a Diaphanous-related formin in integrin traffic. We identify FMNL2 as a target of PKCα-dependent phosphorylation, which controls the impact of FMNL2 on β1-integrin function by regulating its activity and subcellular localization. Our findings provide a mechanistic understanding on how FMNL2 upregulation drives cancer cell motility.

RESULTS

FMNL2 Is Required for β1-Integrin Internalization and Is Phosphorylated by PKCα at Serine 1072

As endocytosis involves the passage of membrane vesicles through the rigid actin cortex and as formins are essential for actin assembly, we hypothesized that formins may be involved in integrin endocytosis. We conducted a β1-integrin endocytosis

RNAi screen employing the cell spot microarray platform (Pellinen et al., 2012; Rantala et al., 2011a) targeting human formins with small interfering RNA (siRNA) doublets. Silencing of FMNL2 led to a decrease in β1-integrin endocytosis in HeLa cells, with two independent siRNAs (Figure S1A). Similar results were obtained in MDA-MB-231 cells (data not shown). To confirm the requirement of FMNL2 for integrin endocytosis, we performed biotin-IP-based β1-integrin endocytosis assays in HeLa cells stably expressing shFMNL2 or control small hairpin RNA (shRNA). Indeed, suppression of FMNL2 significantly inhibited β1-integrin endocytosis at 15 and 30 min time points (Figures 1A and S1B), arguing for the importance of FMNL2 in β1-integrin internalization.

Analyzing the amino acid sequence of FMNL2, we found that it is abundant in basic residues in its DAD region, whereby a conserved serine at position 1072 within a RRSVR (R, Arg; S, Ser; V, Val) motif (Figure 1B) constitutes a potential target for classical PKCs (Nishikawa et al., 1997) previously implicated in β1-integrin trafficking (Ng et al., 1999; Upla et al., 2004). PKCs containing a regulatory C1 domain for diacylglycerol (DAG) binding translocate from the cytosol to membrane compartments and become activated upon 12-O-tetradecanoylphorbol-13-acetate (TPA) stimulation (Rosse et al., 2010). To identify whether FMNL2 is a direct target for PKCs, we immunoprecipitated epitope-tagged FMNL2 for analysis with anti-phospho-Ser PKC substrate antibodies. Upon TPA induced activation of PKC, we observed robust phosphorylation of FMNL2 that was abrogated in the presence of the PKC inhibitor bisindolylmaleimide I (BIM-1) (Grodsky et al., 2006) (Figure 1C). We then generated an FMNL2-S1072A mutant targeting the potential phosphorylation site S1072. Interestingly, mutation of S1072 abolished phosphorylation of FMNL2 (Figure 1C). In addition, PKC-mediated modification appeared to be specific for FMNL2, as the Diaphanous-related formin mDia1 lacked detectable phosphorylation (Figure 1C). FMNL2 was phosphorylated to a similar level regardless of the type or the position of the epitope tag (N- or C-terminal; Figure S1C), and phosphorylation was observed for endogenous FMNL2 as well (Figure 1D). S1072 phosphorylation was dose dependent with TPA concentrations as low as 5 nM being sufficient for full FMNL2 phosphorylation (Figure 1E).

The PKC family consists of ten isozymes classified into three groups: classical (PKCα, PKCβI, PKCβII, PKCγ), novel (PKCδ, PKCε, PKCη, PKCθ), and atypical (PKCζ, PKCλ/ι) PKCs. Individual PKCs have distinct roles in proliferation, apoptosis, cell survival, and migration (Rosse et al., 2010). In order to assess which isozyme is responsible for FMNL2 phosphorylation, we performed in vitro kinase assays and found that, among the 10 human PKC isozymes, PKCα, PKCβI, PKCβII, and PKCδ were active against the FMNL2 peptide, provided it carried a serine at position 1072 (Figure S1F). To understand the specific and physiological role of PKC-mediated FMNL2 phosphorylation in cells, we silenced PKCα, PKCβ, PKCδ, and PKCε (PKCζ was included as a control) and determined FLAG-FMNL2 phosphorylation following immunoprecipitation from cell lysates. Specifically silencing of PKCα resulted in a significant reduction of phosphorylated FMNL2 also when cells were stimulated with TPA (Figures 1F, 1G, S1D, and S1E), indicating that PKCα is the dominant isozyme that specifically phosphorylates FMNL2 in cells. This was confirmed using the pharmacological inhibitor Gö6976, which specifically inhibits PKCα and PKCβI activity (Figure S1G). Consistently, a dominant-negative form of PKCα also inhibited FMNL2 phosphorylation, whereas wild-type or a constitutively active form of PKCα robustly increased the amount of phosphorylated FMNL2 (Figure 1H).

To test whether FMNL2 associates with PKCα, we performed coimmunoprecipitation studies and observed that interaction of FMNL2 with PKCα increased when cells were treated with BIM-1 (Figure 1I), suggesting that the ATP-competitive inhibitor BIM-1 locks the kinase domain of PKCα in a conformation favorable for FMNL2 binding.

Next we tested whether PKC impinges on FMNL2 autoinhibition by assessing FMNL2 DID and DAD binding (autoinhibitory complex). GST-HA tandem tagged FMNL2-NT containing the DID region was purified and GST was cleaved. Notably, HA-FMNL2-NT interacted with wild-type as well as S1072A His-FMNL2-CT, but not with the S1072E mutant protein (Figures 1J and S1I). Moreover, FMNL2-FH3 containing the DID region readily coimmunoprecipitated with the C terminus of FMNL2 possessing its DAD domain (F1F2-CT) under control conditions. Interestingly, this interaction was abrogated upon TPA stimulation but remained unaffected when PKC activity was inhibited by BIM-1 (Figure S1H). These data reveal regulation of FMNL2 autoinhibition upon phosphorylation and suggest that PKC-mediated activation and phosphorylation of FMNL2 is specific and dependent on an intact serine 1072.

FMNL2 Rapidly Relocates in a PKCα-Dependent Manner

We previously showed that FMNL2 can be regulated by RhoC (Kitzing et al., 2010). Thus, we tested whether RhoC impacts on FMNL2 phosphorylation and localization by PKC. Expression of C3 transferase abolished TPA-induced FMNL2 phosphorylation, while expression of active RhoC-V14 enhanced FMNL2 phosphorylation under basal conditions (Figures S2A and S2B). As FMNL2 shows plasma membrane localization under control conditions (Figure S2C), we asked whether RhoC plays a role in FMNL2 membrane targeting. Indeed, RhoC suppression by siRNA or C3 treatment inhibited plasma membrane localization of FMNL2 (Figure S2C), while RhoC-V14 delayed relocation of FMNL2 (Figure S2D and see below), suggesting that FMNL2 regulation by RhoC can facilitate its plasma membrane targeting for phosphorylation by PKC.

Since the data above indicate that FMNL2 subcellular localization is a regulated process and plasma membrane translocation of activated PKCs is crucial for their activity toward substrates (Sakai et al., 1997; Steinberg, 2008), we studied the functional consequences of FMNL2 phosphorylation in living cells. As expected, addition of TPA induced rapid and efficient translocation of GFP-PKCα from the cytoplasm to the plasma membrane (Figure 2A). Interestingly, this was mirrored by the simultaneous and rapid disappearance of FMNL2-mCherry from the cortical plasma membrane (Figure 2A; Movie S1). Quantitative analysis of changes in fluorescence intensity over time revealed that PKCα plasma membrane accumulation was accompanied by a departure of FMNL2 from the plasma membrane in response to TPA (Figure 2B). The process of PKCα translocation and FMNL2 relocation was dose dependent (Figure 2C). Consistent with the importance of PKCα-mediated phosphorylation in this

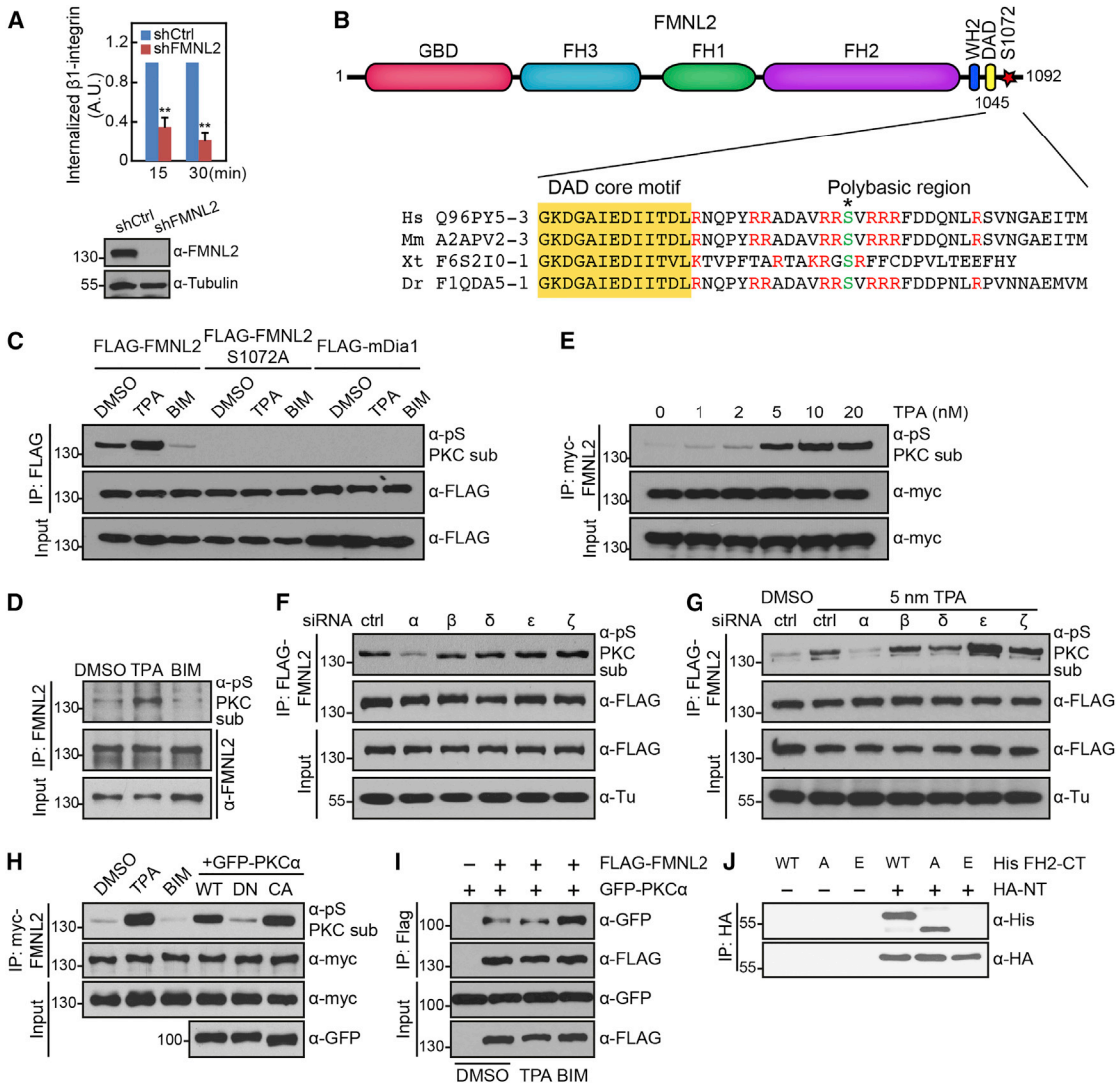

Figure 1. FMNL2 Is Required for β1-Integrin Internalization and Is a Target of PKCα

(A) β1-integrin internalization assays in HeLa cells stably expressing control or FMNL2 shRNA. Internalized integrins were normalized against total. Error bars, +SEM (n = 4); **p < 0.001. Time points indicate time of internalization. Western blot shows knockdown efficiencies.

(B) Schematic of FMNL2 protein. GBD, GTPase binding domain; FH3, formin homology 3 domain; FH1, formin homology 1 domain; FH2, formin homology 2 domain; WH2, WASP homology 2 domain; DAD, diaphanous autoinhibitory domain. Amino acid sequences from different species are shown. Hs, *Homo sapiens*; Mm, *Mus musculus*; Xt, *Xenopus tropicalis*; Dr, *Danio rerio*. Protein IDs are from UniProt. Yellow indicates the DAD core motif. Basic residues are in red. The conserved serine (asterisk) is shown in green.

(C) FLAG-FMNL2, -S1072A, or -mDia1 were immunoprecipitated after DMSO, TPA (20 nM), or BIM (2 μM) treatment for 30 min. An antibody specifically recognizing phospho-(Ser) PKC substrate (α-pS-PKC sub) was used to detect phosphorylated FMNL2.

(D) HeLa cells were treated with DMSO, 20 nM TPA, or 2 μM BIM (30 min) and immunoprecipitated using FMNL2 antibodies following western blot analysis (α-pS-PKC sub).

(E) Titration of TPA-stimulated (30 min) myc-FMNL2 phosphorylation.

(F) HEK293 cells were transfected with FLAG-FMNL2 and siRNA against different PKC isozymes respectively. siPKCβ targets both PKCβI and PKCβII. FLAG-FMNL2 was immunoprecipitated following western blot analysis (α-pS-PKC sub).

(G) HEK293 cells were transfected with FLAG-FMNL2 and siRNA against different PKC isozymes respectively. siPKCβ targets both PKCβI and PKCβII. FLAG-FMNL2 was immunoprecipitated after DMSO or TPA treatment following western blot analysis (α-pS-PKC sub).

(H) myc-FMNL2 was immunoprecipitated from HEK293 cells in the presence or absence of GFP-PKCα wild-type (WT), dominant-negative (DN), or constitutively active (CA) forms following western blot analysis (α-pS-PKC sub). DMSO, 20 nM TPA, or 2 μM BIM was added as indicated.

(I) Immunoprecipitations of HEK293 cells expressing FLAG-FMNL2 and GFP-PKCα after DMSO, 20 nM TPA, or 2 μM BIM treatment. Associated PKCα was detected using anti-GFP antibodies.

(J) Immunoprecipitations were performed with purified HA-FMNL2-NT (15 μg) and His-FMNL2-FH2-CT (30 μg) or the mutants (30 μg).

Molecular weights (kD) are indicated on the left (A and C–J). See also Figure S1.

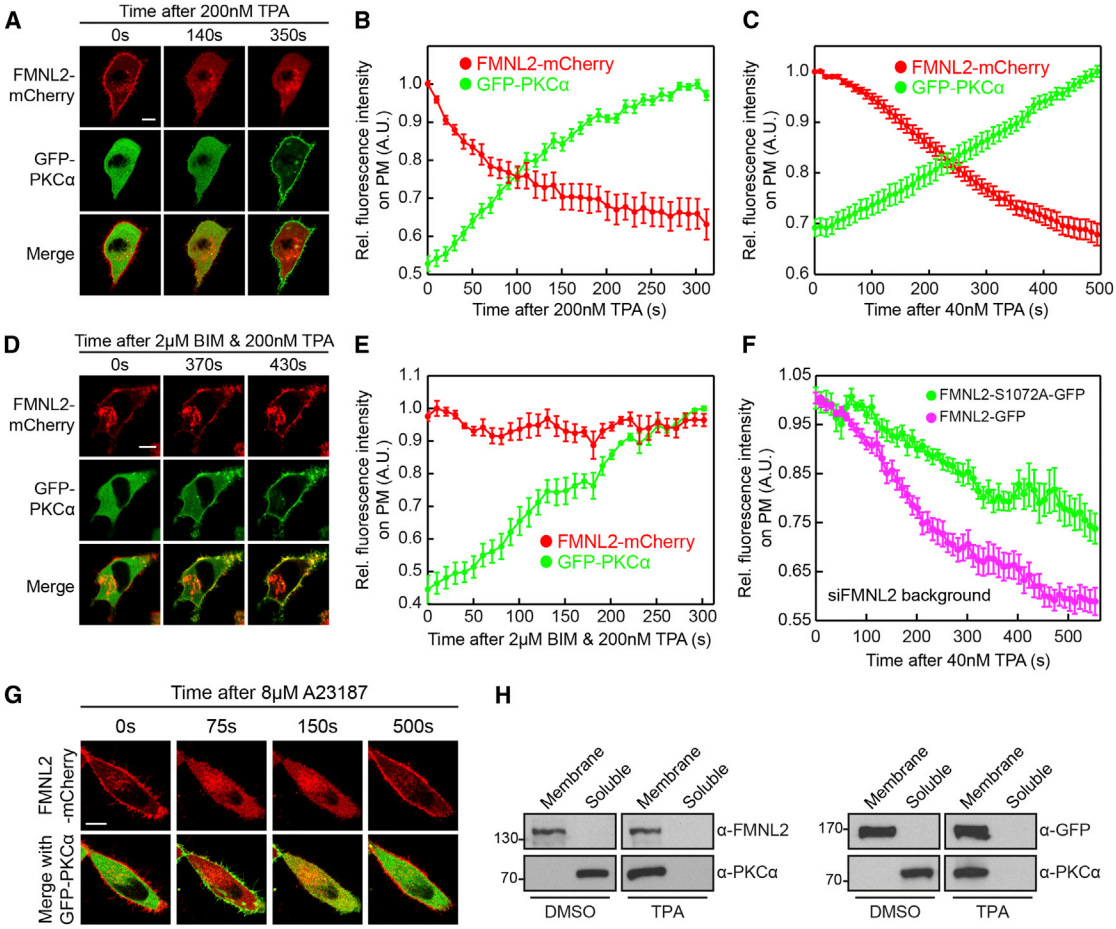

Figure 2. FMNL2 Rapidly Relocates upon PKCα Activation

(A) HeLa cells expressing FMNL2-mCherry and GFP-PKCα were imaged while applying 200 nM TPA. Representative frames are shown at indicated time points. Scale bar, 10 μm. See also Movie S1.

(B) Quantification of fluorescence intensity changes on the plasma membrane for both channels of (A). Red: mCherry. Green: GFP. Error bar, ±SEM of 11 cells.

(C) Quantification of fluorescence intensity changes on the plasma membrane for FMNL2-mCherry and GFP-PKCα during live imaging as in (A) after treating cells with 40 nM TPA. Red: mCherry. Green: GFP. Error bar, ±SEM of nine cells.

(D) HeLa cells expressing FMNL2-mCherry and GFP-PKCα were pre-treated with 2 μM BIM for 30 min. Images were acquired while applying 200 nM TPA. Representative frames are shown. Scale bar, 10 μm. See also Movie S2.

(E) Quantification of fluorescence intensity changes on the plasma membrane for both channels of (D). Red: mCherry. Green: GFP. Error bar, ±SEM of four cells.

(F) Quantification of fluorescence intensity changes on the plasma membrane for the GFP channel in HeLa cells transfected with FMNL2 siRNA labeled with AlexaFluor 555 targeting 3′-UTR. Error bar, ±SEM of eight (FMNL2-S1072A-GFP) and nine (FMNL2-GFP) cells, respectively.

(G) HeLa cells expressing FMNL2-mCherry and GFP-PKCα were imaged while applying 8 μM calcium ionophore A23187. Representative images are shown. See also Movie S3. Scale bar, 10 μm.

(H) HeLa (left) or HEK293 (right) cells were fractionated by membrane flotation assay with DMSO or 200 nM TPA treatment for 30 min. HEK293 cells were transfected with FMNL2-GFP. Membrane and soluble fractions were analyzed using antibodies as indicated. Numbers indicate molecular weights (kD). See also Figure S2.

process, we observed that TPA-induced FMNL2 relocation was blocked by addition of the PKC inhibitor BIM-1, which did not affect the translocation of PKCα (Figures 2D and 2E; Movie S2).

To address the real-time membrane dynamics of the non-phosphorylatable FMNL2-S1072A mutant without interference from the endogenous protein due to homodimerization (Vaillant et al., 2008) (Figure S2E), we suppressed FMNL2 expression using fluorescently labeled siRNAs targeting the 3′-UTR (Figure S2F), and we re-expressed FMNL2-GFP or FMNL2-S1072A-GFP (Figure S2G). Interestingly, FMNL2-S1072A-GFP still relocated but with significantly slower kinetics as compared to FMNL2-GFP (Figures 2F and S2G). FMNL2-S1072E-GFP kinetics was similar to FMNL2-S1072A-GFP (Figures S2H and S2G). Thus, phosphorylation of FMNL2 and an intact S1072 residue are crucial to maintain proper spatiotemporal dynamics for FMNL2 relocation.

While its activation by TPA is permanent and irreversible, PKC activation by DAG in cells is transient (Sakai et al., 1997; Steinberg, 2008). Thus we used the calcium ionophore A23187 to

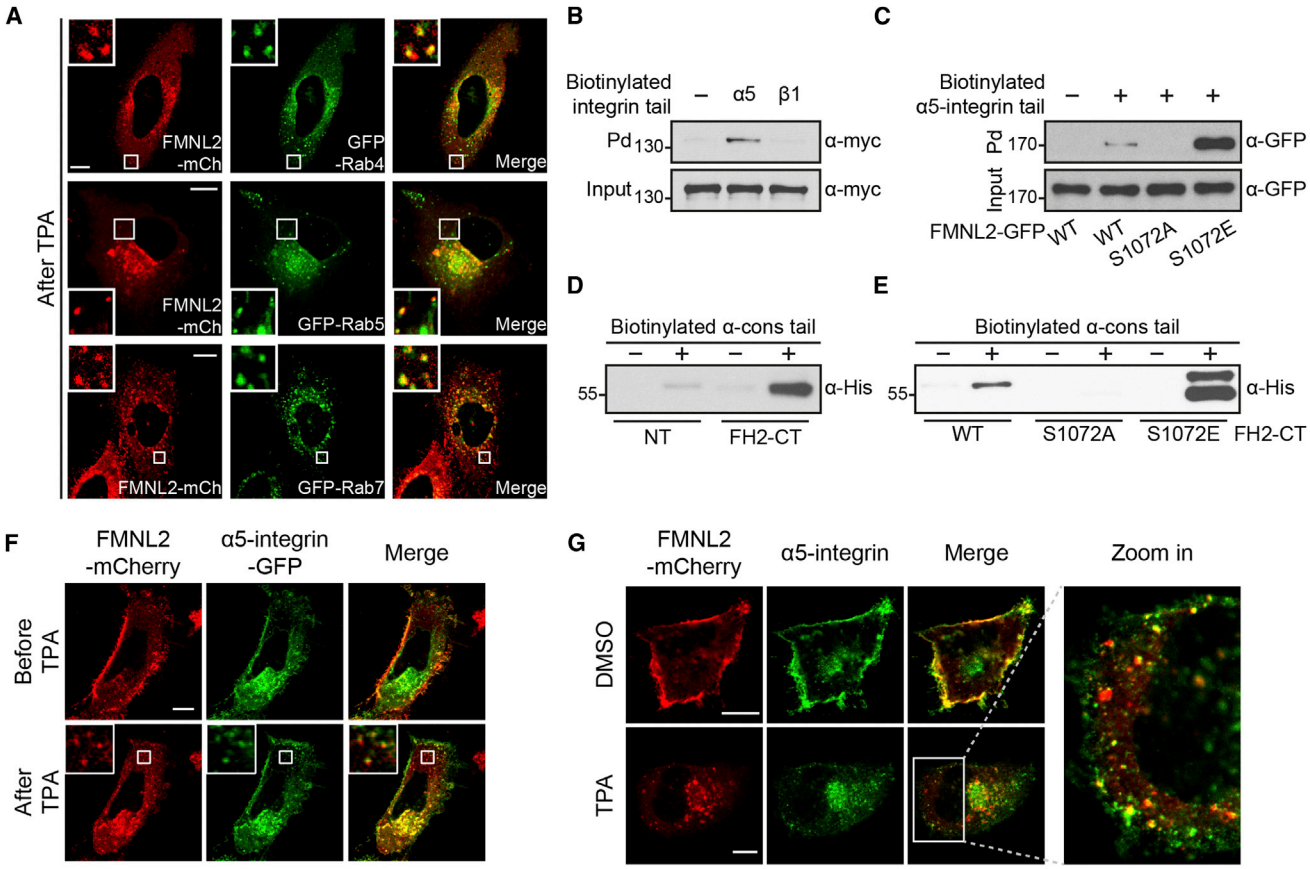

Figure 3. FMNL2 Interacting with α-Integrin Depends on PKCα Activation

(A) Representative images of FMNL2-mCherry (red) and GFP-Rabs (green) in HeLa cells after 200 nM TPA treatment for 20 min. Scale bars, 10 μm.

(B) Biotin-streptavidin pull down (Pd) of integrin cytoplasmic tails from HEK293 cell extracts expressing FMNL2-myc.

(C) Biotin-streptavidin pull down (Pd) of α5-integrin cytoplasmic tail from HEK293 cell extracts expressing FMNL2-GFP constructs.

(D) Biotin-streptavidin pull down (Pd) of α-integrin conserved cytoplasmic tails and His-FMNL2-NT or His-FMNL2-FH2-CT (30 μg each).

(E) Biotin-streptavidin pull down (Pd) of α-integrin conserved cytoplasmic tails and His-FMNL2-FH2-CT, or its mutants (30 μg each). Numbers indicate the molecular weights in the western blots (B–E).

(F) FMNL2-mCherry and α5-integrin-GFP were expressed in HeLa cells, and 200 nM TPA was applied to cells at time point zero. Representative images are shown. Scale bar, 10 μm. See also Movie S4.

(G) FMNL2-mCherry and endogenous α5-integrin localization with or without 200 nM TPA treatment for 20 min. Scale bars, 10 μm. See also Figure S3.

transiently activate classical PKC isozymes including PKCα and monitored FMNL2 and PKCα dynamics over time. Upon addition of 8 μM A23187, GFP-PKCα translocated to the plasma membrane followed by rapid FMNL2-mCherry redistribution into the cytoplasm (Figure 2G). PKCα gradually translocated from the plasma membrane back to the cytoplasm within 150 s, indicating kinase inactivation. Consistent with PKCα inactivation, FMNL2 plasma membrane localization was fully recovered after 500 s (Figure 2G; Movie S3).

To explore whether FMNL2 remains attached to cellular membranes during relocation, we separated cell lysates into cytosolic (soluble) and membrane fractions by flotation analysis (Pan et al., 2012). PKCα shifted from the soluble to the membrane fraction in response to TPA as expected (Figure 2H). In contrast, endogenous FMNL2 or FMNL2-GFP remained membrane associated, arguing that PKCα activation triggers FMNL2 relocation into intracellular membranes (Figure 2H). This is in agreement with the fact that FMNLs are N-terminally myristoylated for efficient membrane interactions (Han et al., 2009; Moriya et al., 2012).

FMNL2 Relocates to Endosomal Membrane Compartments in Response to PKCα Activation

To better characterize the intracellular membrane compartments associated with FMNL2, we transiently expressed FMNL2-mCherry together with the endosome markers Rab4-GFP, Rab5-GFP, and Rab7-GFP. Upon TPA treatment, the majority of FMNL2 was found to colocalize with the early endosome markers Rab4 and Rab5 and with the late endosome marker Rab7 (Figure 3A). Colocalizations were quantified for Rab4, Rab5, or Rab7 under DMSO or TPA treated conditions. FMNL2 colocalization with Rab4, Rab5, or Rab7 was significantly elevated when cells were stimulated with TPA (Figure S3A). Further, we found no significant colocalizations between FMNL2-mCherry and the ER marker (PDI) or Golgi marker (GM130 and TGN38-YFP) (Figures S3B, S3C, and S3D). These

data indicate that FMNL2 relocates to endosomal membranes upon activation by PKCα.

FMNL2 Phosphorylation Mediates Binding to α-Integrin Cytoplasmic Tail for Integrin Internalization and Cell Invasion

Since FMNL2 was shown to regulate β1-integrin internalization and localize to endosomal membranes upon PKCα activation, we performed biotin-streptavidin pull-down assays using synthesized biotinylated α5- or β1-integrin tail peptides and found that FMNL2 specifically bound the α5-, but not the β1-integrin, tail (Figure 3B). This was confirmed by immunoprecipitation in α5-integrin-GFP expressing cells (Figure S3E). Notably, the non-phosphorylatable FMNL2-S1072A mutant was unable to interact with α5-integrin, while the phospho-mimetic FMNL2-S1072E displayed enhanced binding to the α5-integrin tail (Figures 3C and S3F).

Next, FMNL2-NT (containing the GBD and FH3 domains) and FH2-CT (containing the FH2 and DAD domains) were purified and tested for direct interaction with a peptide containing the conserved membrane proximal sequence found in all α-integrin subunits that hetero-dimerize with β1-integrin (Rantala et al., 2011b). While FMNL2-NT interacted weakly, FMNL2-FH2-CT interacted strongly with the α-tail peptide (Figures 3D and S3G). Importantly, the interaction between FMNL2-CT and the integrin α-tail depended on the phosphorylation status of the S1072 residue (Figure 3E) since addition of the α-tail peptide was able to partially release interaction between FMNL2-NT and FMNL2-FH2-CT (Figure S3H). These data suggest that FMNL2 regulates α/β1-integrin heterodimer internalization through direct interaction with the α-integrin tail and that FMNL2/α-integrin interaction is dynamically and tightly regulated through its phosphorylation by PKCα.

Next we assessed whether FMNL2 localizes to α5-integrin positive vesicles. Cells transiently expressing FMNL2-mCherry and α5-integrin-GFP were analyzed for colocalization in intracellular vesicles in response to TPA stimulation. Indeed, FMNL2 appeared to co-traffic and subsequently colocalize with α5-integrin-GFP vesicles (Figure 3F; Movie S4). Importantly, FMNL2-mCherry colocalized with endogenous α5-integrin vesicles in response to TPA (Figures 3G and S3I), suggesting that both proteins associate in intracellular vesicles upon PKCα activation.

We then asked whether FMNL2 regulates the internalization of distinct α/β1-integrins. Indeed, silencing of FMNL2 strongly attenuated internalization of α5β1-integrin (Figures 4A and S4A) as well as α2β1-integrin (Figures 4B and S4B). This was specific for integrins since transferrin receptor (TfR) internalization was not dependent on FMNL2 (Figures 4C and S4B). This effect was not due to reduced cell surface integrin levels, since loss of FMNL2 increased integrin cell surface levels (Figure S4D). Hence, FMNL2 regulates endocytosis of α/β1-integrin heterodimers owing to its ability to interact with the α-tail conserved sequence in a phosphorylation-dependent manner.

As expected, TPA-mediated PKC activation increased β1-integrin internalization and β1-integrin endocytosis was sensitive to PKC inhibition (Figures 4D and S4C). Notably, the influence of PKC on β1-integrin internalization was FMNL2 dependent (Figures 4D and S4C). To further investigate the effects of FMNL2 phosphorylation and actin assembly on β1-integrin, we tracked surface β1-integrin by an imaging-based endocytosis assay (Gu et al., 2011) in FMNL2-silenced cells in which phospho-insensitive (S1072A), phospho-mimetic (S1072E) or actin assembly-defective (ILI3A: I704A, L1028A, and I1029A; Figures S4E and S4F) mutants were re-introduced. These analyses show that FMNL2 overexpression results in enhanced β1-integrin internalization (Figures 4E and S4G). However, re-expression of the non-phosphorylatable or actin-binding deficient FMNL2 mutants significantly interfered with β1-integrin endocytosis (Figure 4E), demonstrating that dynamic phospho-regulation and FMNL2-dependent actin assembly are necessary for β1-integrin internalization. In addition, FMNL2 significantly affected α2- and α5-integrin endocytosis, consistent with its ability to interact with both α-integrin subunits (Figures S4H and S4I).

Next we investigated the impact of FMNL2 and its regulation by S1072 phosphorylation on cancer cell invasion. We used A375M2 melanoma cells (Sahai and Marshall, 2003) to generate cell lines stably expressing FMNL2-S1072A, FMNL2-S1072E, FMNL2-ILI3A, or wild-type FMNL2 and analyzed their migratory potentials through a fibronectin-containing matrix. Notably, wild-type FMNL2 robustly promoted cell invasion, which was RhoC dependent and PKC dependent (Figure 4F). In contrast, cells expressing FMNL2-S1072A or FMNL2-S1072E failed to significantly induce invasive migration, while the mutant deficient for actin assembly inhibited invasion (Figure 4F). Thus, FMNL2 may have important roles for invasive cancer cell migration not only through regulating integrin trafficking but also via additional actin-mediated functions (Kitzing et al., 2010). Thus, dynamic regulation of FMNL2 by PKCα-mediated phosphorylation represents a critical mechanism for cancer cell migration that could be pharmacologically targeted.

DISCUSSION

Here we identified a role for the actin assembly factor FMNL2 in β1-integrin trafficking. Cortical membrane associated FMNL2 rapidly and reversibly undergoes relocation upon activation by PKCα, resembling a so far unique property of a mammalian formin. Thus, subcellular distribution of FMNL2 is very dynamic and signal regulated. We demonstrate that PKCα phosphorylates the FMNL2 C terminus to control its localization and autoinhibition, thus uncovering a mode of formin activation by PKCs. In addition, PKCα-mediated S1072 phosphorylation of FMNL2 involves RhoC, indicating a more complex regulation of FMNL2 for spatiotemporal activation. Hence, FMNL2 interaction with RhoC may help to facilitate the accessibility of FMNL2-S1072 for PKCα to drive β1-integrin endocytosis, which is in agreement with a study showing that RhoC associates with α5β1-integrin to promote its internalization in migrating carcinoma cells (Li et al., 2013).

We observed rapid relocation of FMNL2 from the cell cortex upon PKCα activation. However, while pharmacological inhibition of PKC abolishes FMNL2 relocation, mutating the FMNL2 residue S1072 did not block the process per se but made it significantly slower, suggesting that relocation kinetics are critical for proper cellular output. Indeed, our data show that relocation of FMNL2 to endocytic membranes upon activation of PKCα is a reversible process that enables cells to rapidly and precisely respond to extracellular cues.

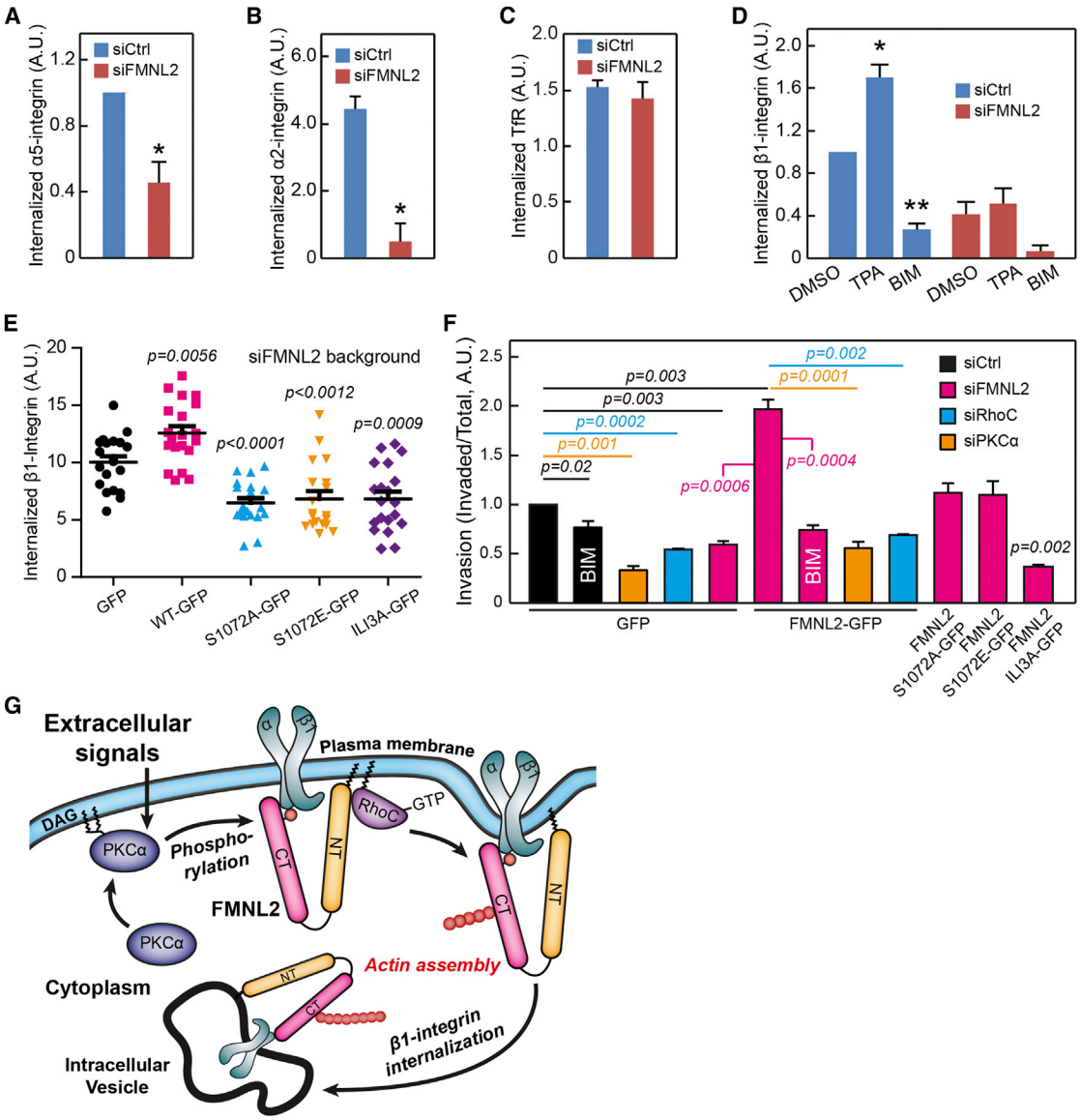

Figure 4. PKCα Promotes FMNL2 to Drive β1-Integrin Internalization and Cancer Cell Invasion

(A) Biotin-IP based internalization assays show α5-integrin internalization in HeLa cells at time point 30 min. Internalized proteins were normalized against the total. Error bars, +SEM (n = 3); *p < 0.05.

(B) Biotin-IP based internalization assays show α2-integrin internalization in HeLa cells at time point 30 min. Internalized proteins were normalized against the total. Error bars, +SEM (n = 3); *p < 0.05.

(C) Biotin-IP based internalization assays show TfR (transferrin receptor) internalization in HeLa cells at time point 30 min. Internalized proteins were normalized against the total. Error bars, +SEM (n = 3).

(D) Biotin-IP based β1-integrin internalization assays were performed in control or FMNL2 silenced cells at time point 30 min, with either DMSO, 200 nM TPA, or 2 μM BIM-1 treatment. Internalized integrins were normalized against the total. Error bars: +SEM (n = 3); *p < 0.05, **p < 0.001.

(E) Quantified levels of internalized β1-integrin in HeLa cells expressing GFP, or GFP-tagged FMNL2 mutants under endogenous FMNL2 silenced background by imaging-based endocytosis assays. The graph shows mean line with error bar, +SEM (n = 4). Each point presents mean value of endocytosed β1-integrin in one field of view. In total, 100–150 cells were measured per group. Indicated p values are compared to the GFP control.

(F) Inverted transwell Matrigel (containing 100 μg/ml fibronectin) invasion of A375M2 cells stably expressing GFP or GFP-tagged FMNL2 mutants were transfected with siRNAs. 2 μM BIM was used when indicated. The percentage of invaded cell over the total cell number was quantified and normalized. Error bar, +SD. (n = 3). p values are indicated with straight lines except for FMNL2-ILI3A, which was compared to the GFP with siFMNL2.

(G) Model of PKCα-mediated FMNL2 phosphorylation and subsequent β1-integrin internalization. See also Figure S4.

PKCα has been implicated in β1-integrin trafficking (Ng et al., 1999), while cell motility requires tight control of β1-integrin cell surface turnover through endocytic routes (Caswell and Norman, 2008; Cheng et al., 2004; Ivaska et al., 2002; Muller et al., 2009). Our data support a model in which PKCα phosphorylates FMNL2 for release of autoinhibition and binding to the α-integrin tail as

well as localization into α5-integrin positive vesicles, revealing a dynamic signal-regulated complex for actin-dependent α/β1-integrin endocytosis (Figure 4G). However, both the non-phosphorylatable and the phospho-mimetic FMNL2 mutant interfered with β1-integrin internalization, suggesting that phosphorylation of FMNL2 may play a critical role as a molecular "switch" to steer and tightly coordinate β1-integrin trafficking for invasive migration. As FMNL2 is also involved in epithelialization (Grikscheit et al., 2015), it is conceivable that during cancer progression FMNL2 regulation becomes altered from cell-cell to cell-matrix adhesion. Further work is needed to address this.

Together, our data show that a member of the formin family is a target of PKC to regulate β1-integrin traffic and function, making this mechanism an attractive target for therapeutic intervention.

EXPERIMENTAL PROCEDURES

Internalization Assay

Integrin or transferrin receptor (TfR) internalization assays were performed as described (Pellinen et al., 2008).

Live Cell Imaging and Analysis of Fluorescence Intensity

Coverslips seeded with cells were inserted into a customized imaging dish and mounted to the microscope objective. Live cell imaging was performed at 37°C, in a CO_2 chamber. Images were acquired every 5 to 10 s with a LSM 700 confocal microscope (Zeiss), using the 63X/1.4 oil objective. Drugs were applied to the cells at the microscope while scanning. Different channels were scanned sequentially by line.

2D fluorescence intensity images with time stamps were segmented by Sobel edge detection with building function in MATLAB to identify the plasma membrane region. Fluorescence intensities were summed up for each cell and normalized by their maximum intensity. Photo bleaching was corrected by keeping the overall intensity of the whole cell constant. Statistics were given on the normalized fluorescence intensity at each time point.

Imaging-Based Integrin Endocytosis Assay

Cells were transfected with QIAGEN Hs_FMNL2_9 siRNA (targeting 3′UTR) and EGFP or different FMNL2-GFP plasmids. Endocytosis was carried out as described with modifications (Gu et al., 2011).

Inverted Transwell Invasion Assay and Image Analysis

Invasion assays were performed as described (Kitzing et al., 2010). For fixed cell samples, images were obtained with LSM 700 (Zeiss) and then processed with ImageJ. Pearson's correlation coefficient for colocalization was obtained by MATLAB.

For more details, see the Supplemental Experimental Procedures.

SUPPLEMENTAL INFORMATION

Supplemental Information includes Supplemental Experimental Procedures, four figures, and four movies and can be found with this article online at http://dx.doi.org/10.1016/j.devcel.2015.06.015.

ACKNOWLEDGMENTS

We thank D. Richardson for GFP-Rab plasmids and E. Sahai for the A375M2 cells. We thank members of our laboratories, A. Ridley and H.N. Higgs for helpful discussions, B. Di Ventura for reading, and H. Hamidi for editing of our manuscript as well as T. Hofmann and M. Losekam for technical assistance. This work was supported by grants from the DFG (GR2111/2-2 to R.G.), the Wilhelm Sander Stiftung (2013.149.1 to R.G.), the Deutsche Krebshilfe (grant 109550 to R.G. and O.T.F.), the Academy of Finland ERC Consolidator Grant, the Sigrid Juselius Foundation, and the Finnish Cancer Organization (to J.I.). P.P. is an IMPRS-Mic fellow.

Received: March 31, 2014
Revised: April 1, 2015
Accepted: June 18, 2015
Published: August 6, 2015

REFERENCES

Baarlink, C., Brandt, D., and Grosse, R. (2010). SnapShot: Formins. Cell *142*, 172–172.e1.

Bass, M.D., Williamson, R.C., Nunan, R.D., Humphries, J.D., Byron, A., Morgan, M.R., Martin, P., and Humphries, M.J. (2011). A syndecan-4 hair trigger initiates wound healing through caveolin- and RhoG-regulated integrin endocytosis. Dev. Cell *21*, 681–693.

Brandt, D.T., Marion, S., Griffiths, G., Watanabe, T., Kaibuchi, K., and Grosse, R. (2007). Dia1 and IQGAP1 interact in cell migration and phagocytic cup formation. J. Cell Biol. *178*, 193–200.

Breitsprecher, D., and Goode, B.L. (2013). Formins at a glance. J. Cell Sci. *126*, 1–7.

Caswell, P., and Norman, J. (2008). Endocytic transport of integrins during cell migration and invasion. Trends Cell Biol. *18*, 257–263.

Caswell, P.T., Chan, M., Lindsay, A.J., McCaffrey, M.W., Boettiger, D., and Norman, J.C. (2008). Rab-coupling protein coordinates recycling of α5β1 integrin and EGFR1 to promote cell migration in 3D microenvironments. J. Cell Biol. *183*, 143–155.

Cheng, K.W., Lahad, J.P., Kuo, W.L., Lapuk, A., Yamada, K., Auersperg, N., Liu, J., Smith-McCune, K., Lu, K.H., Fishman, D., et al. (2004). The RAB25 small GTPase determines aggressiveness of ovarian and breast cancers. Nat. Med. *10*, 1251–1256.

De Franceschi, N., Hamidi, H., Alanko, J., Sahgal, P., and Ivaska, J. (2015). Integrin traffic - the update. J. Cell Sci. *128*, 839–852.

Faix, J., and Grosse, R. (2006). Staying in shape with formins. Dev. Cell *10*, 693–706.

Grikscheit, K., Frank, T., Wang, Y., and Grosse, R. (2015). Junctional actin assembly is mediated by Formin-like 2 downstream of Rac1. J. Cell Biol. *209*, 367–376.

Grodsky, N., Li, Y., Bouzida, D., Love, R., Jensen, J., Nodes, B., Nonomiya, J., and Grant, S. (2006). Structure of the catalytic domain of human protein kinase C βii complexed with a bisindolylmaleimide inhibitor. Biochemistry *45*, 13970–13981.

Gu, Z., Noss, E.H., Hsu, V.W., and Brenner, M.B. (2011). Integrins traffic rapidly via circular dorsal ruffles and macropinocytosis during stimulated cell migration. J. Cell Biol. *193*, 61–70.

Han, Y., Eppinger, E., Schuster, I.G., Weigand, L.U., Liang, X., Kremmer, E., Peschel, C., and Krackhardt, A.M. (2009). Formin-like 1 (FMNL1) is regulated by N-terminal myristoylation and induces polarized membrane blebbing. J. Biol. Chem. *284*, 33409–33417.

Iskratsch, T., Yu, C.-H., Mathur, A., Liu, S., Stévenin, V., Dwyer, J., Hone, J., Ehler, E., and Sheetz, M. (2013). FHOD1 is needed for directed forces and adhesion maturation during cell spreading and migration. Dev. Cell *27*, 545–559.

Ivaska, J., Whelan, R.D.H., Watson, R., and Parker, P.J. (2002). PKC ε controls the traffic of β1 integrins in motile cells. EMBO J. *21*, 3608–3619.

Jacquemet, G., Green, D.M., Bridgewater, R.E., von Kriegsheim, A., Humphries, M.J., Norman, J.C., and Caswell, P.T. (2013). RCP-driven α5β1 recycling suppresses Rac and promotes RhoA activity via the RacGAP1-IQGAP1 complex. J. Cell Biol. *202*, 917–935.

Kaksonen, M., Toret, C.P., and Drubin, D.G. (2006). Harnessing actin dynamics for clathrin-mediated endocytosis. Nat. Rev. Mol. Cell Biol. *7*, 404–414.

Kitzing, T.M., Sahadevan, A.S., Brandt, D.T., Knieling, H., Hannemann, S., Fackler, O.T., Grosshans, J., and Grosse, R. (2007). Positive feedback between Dia1, LARG, and RhoA regulates cell morphology and invasion. Genes Dev. *21*, 1478–1483.

Kitzing, T.M., Wang, Y., Pertz, O., Copeland, J.W., and Grosse, R. (2010). Formin-like 2 drives amoeboid invasive cell motility downstream of RhoC. Oncogene *29*, 2441–2448.

Li, Y., Zhu, X., Zeng, Y., Wang, J., Zhang, X., Ding, Y.Q., and Liang, L. (2010). FMNL2 enhances invasion of colorectal carcinoma by inducing epithelial-mesenchymal transition. Mol. Cancer Res. *8*, 1579–1590.

Li, N.F., Gemenetzidis, E., Marshall, F.J., Davies, D., Yu, Y., Frese, K., Froeling, F.E.M., Woolf, A.K., Feakins, R.M., Naito, Y., et al. (2013). RhoC interacts with integrin α5β1 and enhances its trafficking in migrating pancreatic carcinoma cells. PLoS ONE *8*, e81575.

Liang, L., Li, X., Zhang, X., Lv, Z., He, G., Zhao, W., Ren, X., Li, Y., Bian, X., Liao, W., et al. (2013). MicroRNA-137, an HMGA1 target, suppresses colorectal cancer cell invasion and metastasis in mice by directly targeting FMNL2. Gastroenterology *144*, 624–635.e4.

Moriya, K., Yamamoto, T., Takamitsu, E., Matsunaga, Y., Kimoto, M., Fukushige, D., Kimoto, C., Suzuki, T., and Utsumi, T. (2012). Protein N-myristoylation is required for cellular morphological changes induced by two formin family proteins, FMNL2 and FMNL3. Biosci. Biotechnol. Biochem. *76*, 1201–1209.

Muller, P.A.J., Caswell, P.T., Doyle, B., Iwanicki, M.P., Tan, E.H., Karim, S., Lukashchuk, N., Gillespie, D.A., Ludwig, R.L., Gosselin, P., et al. (2009). Mutant p53 drives invasion by promoting integrin recycling. Cell *139*, 1327–1341.

Ng, T., Shima, D., Squire, A., Bastiaens, P.I.H., Gschmeissner, S., Humphries, M.J., and Parker, P.J. (1999). PKCalpha regulates β1 integrin-dependent cell motility through association and control of integrin traffic. EMBO J. *18*, 3909–3923.

Nishikawa, K., Toker, A., Johannes, F.-J., Songyang, Z., and Cantley, L.C. (1997). Determination of the specific substrate sequence motifs of protein kinase C isozymes. J. Biol. Chem. *272*, 952–960.

Pan, X., Rudolph, J.M., Abraham, L., Habermann, A., Haller, C., Krijnse-Locker, J., and Fackler, O.T. (2012). HIV-1 Nef compensates for disorganization of the immunological synapse by inducing trans-Golgi network-associated Lck signaling. Blood *119*, 786–797.

Pellinen, T., Tuomi, S., Arjonen, A., Wolf, M., Edgren, H., Meyer, H., Grosse, R., Kitzing, T., Rantala, J.K., Kallioniemi, O., et al. (2008). Integrin trafficking regulated by Rab21 is necessary for cytokinesis. Dev. Cell *15*, 371–385.

Pellinen, T., Rantala, J.K., Arjonen, A., Mpindi, J.-P., Kallioniemi, O., and Ivaska, J. (2012). A functional genetic screen reveals new regulators of β1-integrin activity. J. Cell Sci. *125*, 649–661.

Rantala, J.K., Mäkelä, R., Aaltola, A.-R., Laasola, P., Mpindi, J.-P., Nees, M., Saviranta, P., and Kallioniemi, O. (2011a). A cell spot microarray method for production of high density siRNA transfection microarrays. BMC Genomics *12*, 162.

Rantala, J.K., Pouwels, J., Pellinen, T., Veltel, S., Laasola, P., Mattila, E., Potter, C.S., Duffy, T., Sundberg, J.P., Kallioniemi, O., et al. (2011b). SHARPIN is an endogenous inhibitor of β1-integrin activation. Nat. Cell Biol. *13*, 1315–1324.

Rosse, C., Linch, M., Kermorgant, S., Cameron, A.J.M., Boeckeler, K., and Parker, P.J. (2010). PKC and the control of localized signal dynamics. Nat. Rev. Mol. Cell Biol. *11*, 103–112.

Sahai, E., and Marshall, C.J. (2003). Differing modes of tumour cell invasion have distinct requirements for Rho/ROCK signalling and extracellular proteolysis. Nat. Cell Biol. *5*, 711–719.

Sakai, N., Sasaki, K., Ikegaki, N., Shirai, Y., Ono, Y., and Saito, N. (1997). Direct visualization of the translocation of the γ-subspecies of protein kinase C in living cells using fusion proteins with green fluorescent protein. J. Cell Biol. *139*, 1465–1476.

Schirenbeck, A., Bretschneider, T., Arasada, R., Schleicher, M., and Faix, J. (2005). The Diaphanous-related formin dDia2 is required for the formation and maintenance of filopodia. Nat. Cell Biol. *7*, 619–625.

Seth, A., Otomo, C., and Rosen, M.K. (2006). Autoinhibition regulates cellular localization and actin assembly activity of the diaphanous-related formins FRLalpha and mDia1. J. Cell Biol. *174*, 701–713.

Stastna, J., Pan, X., Wang, H., Kollmannsperger, A., Kutscheidt, S., Lohmann, V., Grosse, R., and Fackler, O.T. (2012). Differing and isoform-specific roles for the formin DIAPH3 in plasma membrane blebbing and filopodia formation. Cell Res. *22*, 728–745.

Steinberg, S.F. (2008). Structural basis of protein kinase C isoform function. Physiol. Rev. *88*, 1341–1378.

Upla, P., Marjomäki, V., Kankaanpää, P., Ivaska, J., Hyypiä, T., Van Der Goot, F.G., and Heino, J. (2004). Clustering induces a lateral redistribution of α 2 β 1 integrin from membrane rafts to caveolae and subsequent protein kinase C-dependent internalization. Mol. Biol. Cell *15*, 625–636.

Vaillant, D.C., Copeland, S.J., Davis, C., Thurston, S.F., Abdennur, N., and Copeland, J.W. (2008). Interaction of the N- and C-terminal autoregulatory domains of FRL2 does not inhibit FRL2 activity. J. Biol. Chem. *283*, 33750–33762.

Zech, T., Calaminus, S.D.J., and Machesky, L.M. (2012). Actin on trafficking: could actin guide directed receptor transport? Cell Adhes. Migr. *6*, 476–481.

Zhu, X.L., Liang, L., and Ding, Y.Q. (2008). Overexpression of FMNL2 is closely related to metastasis of colorectal cancer. Int. J. Colorectal Dis. *23*, 1041–1047.

Zhu, X.L., Zeng, Y.F., Guan, J., Li, Y.F., Deng, Y.J., Bian, X.W., Ding, Y.Q., and Liang, L. (2011). FMNL2 is a positive regulator of cell motility and metastasis in colorectal carcinoma. J. Pathol. *224*, 377–388.

Developmental Cell

Supplemental Information

Formin-like 2 Promotes β1-Integrin Trafficking and Invasive Motility Downstream of PKCα

Ying Wang, Antti Arjonen, Jeroen Pouwels, Haisen Ta, Patrick Pausch, Gert Bange,Ulrike Engel, Xiaoyu Pan,Oliver T. Fackler, Johanna Ivaska, and Robert Grosse

Supplemental Figure S1

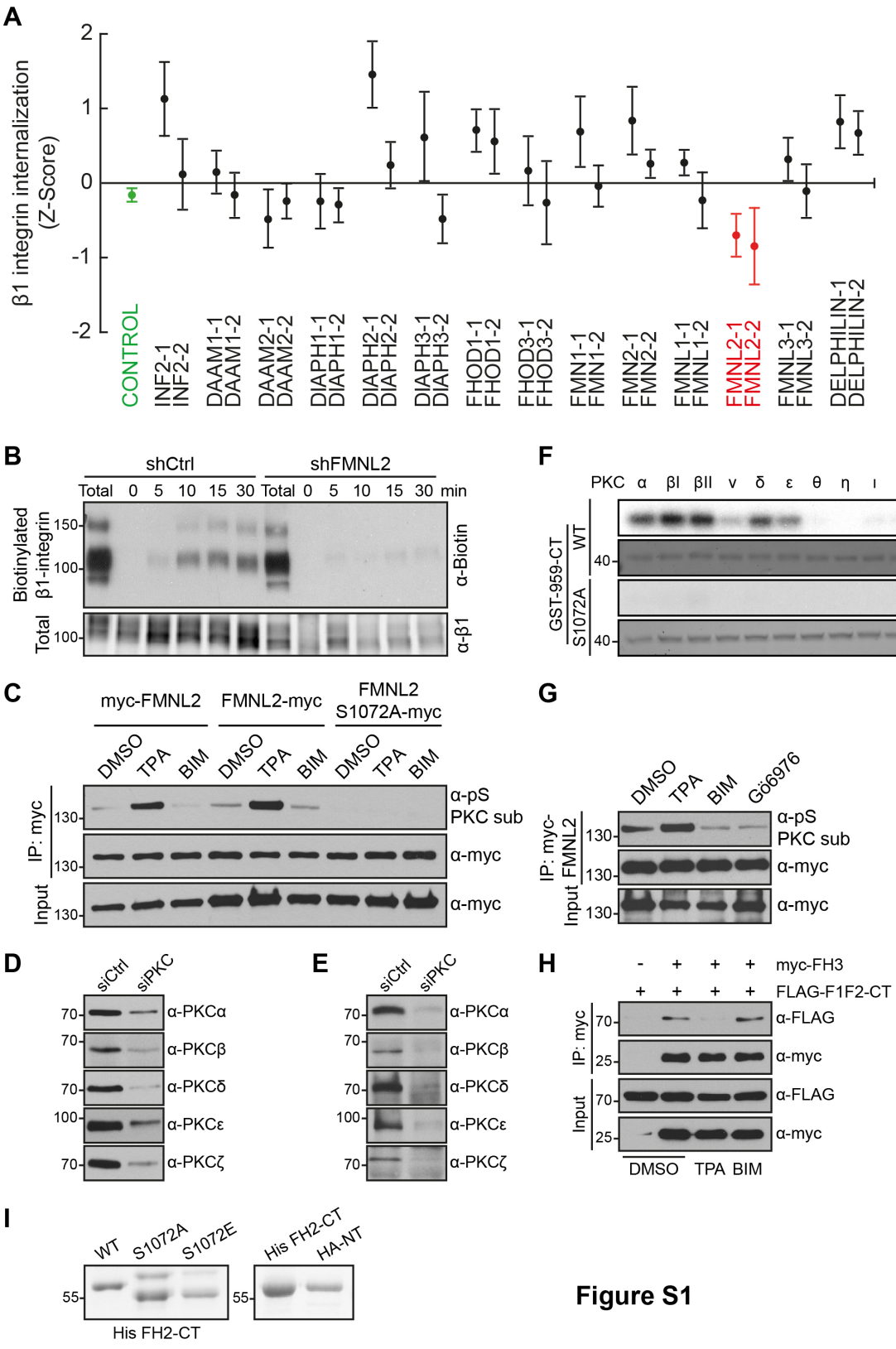

Figure S1

Figure S1. FMNL2 Regulates β1-integrin Endocytosis and Is Phosphorylated by PKCα (Related to Figure 1)

(A) Differential effects of human formins on β1-integrin internalization. After silencing of formin genes, β1-integrin endocytosis was measured using antibody-based β1-integrin endocytosis assay. Endocytosis values are Z-scored among the whole dataset. Error bar: ± SEM (n=6). (B) Representative Western blots showing the immunoprecipitated total β1-integrin or endocytosed biotinylated β1-integrin under shCtrl or shFMNL2 conditions in HeLa cells. (C) myc-FMNL2, FMNL2-myc or FMNL2-S1072A-myc was expressed in HEK293 cells and immunoprecipitated after DMSO, TPA (20 nM) or BIM (2 μM) treatment for 30 min. Phosphorylated FMNL2 was detected by phospho-(Ser) PKC substrate antibody. (D, E) HEK293 cells were transfected with FLAG-FMNL2 and siRNA against different PKC isozymes respectively. siPKCβ targets both PKCβI and PKCβII. Knockdown of different PKC isozymes are shown for Figures 1F and G. (F) In vitro kinase assays using purified PKC isozymes and wild type or S1072A mutant FMNL2 C-terminal fragments (GST-959-CT). Autoradiography and coomassie blue stained gels are shown. (G) HEK293 cells expressing myc-FMNL2 were immunoprecipitated after DMSO, 20 nM TPA, 2 μM BIM or 1 μM Gö6976 treatment. Phosphorylation of FMNL2 by PKC was detected. (H) Immunoprecipitations of HEK293 cells expressing FLAG-FMNL2-F1F2-CT and myc-FMNL2-FH3 after DMSO, 20 nM TPA or 2 μM BIM treatment. (I) Coomassie blue stained gels of the purified proteins used in Figures 1J and 3E. Numbers on the left indicate the molecular weights (kD) (B~I).

Supplemental Figure S2

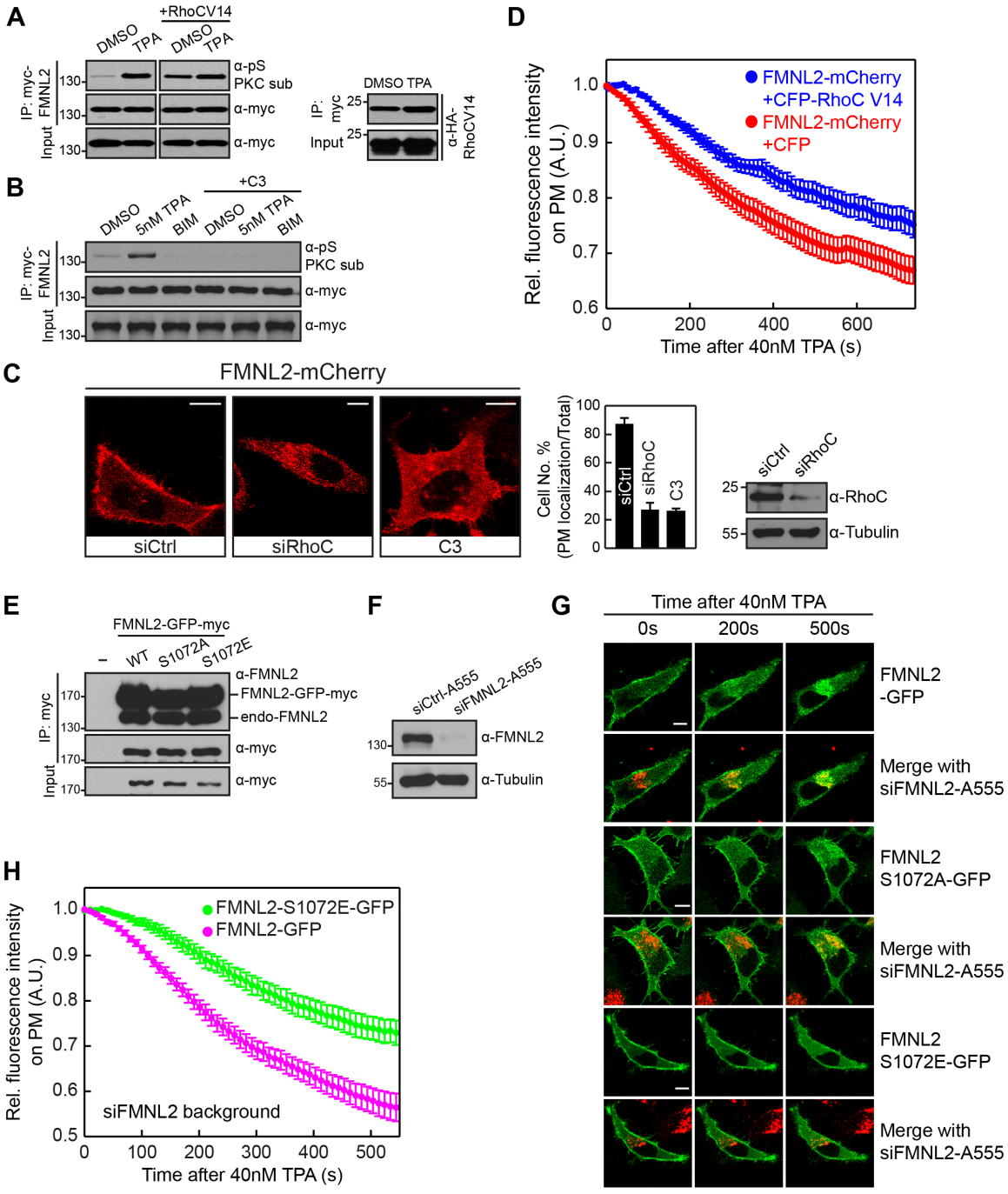

Figure S2

Figure S2. Phosphorylation of FMNL2 Depends on Rho-GTPase Activity and Endogenous FMNL2 Is Knocked-down to Reduce Homodimerization (Related to Figure 2)

(A) FMNL2 and HA-RhoC-V14 were expressed. myc-FMNL2 was immunoprecipitated after DMSO or TPA (20 nM) treatment for 30 min. Phosphorylated FMNL2 and associated HA-RhoCV14 were detected. (B) FMNL2 was co-expressed with or without C3 co-enzyme. myc-FMNL2 was immunoprecipitated after DMSO, TPA (5 nM) or BIM treatment for 30 min. Phosphorylated FMNL2 was detected. (C) FMNL2-mCherry and siCtrl, siRhoC or C3 were co-expressed in HeLa cells. Knockdown of RhoC is shown. Cells expressing FMNL2-mCherry with plasma membrane localization were quantified over the total cell number (in total more than 72 cells per group) counted. Scale bars: 10 μm. Error bar, + SEM (n=3). (D) Quantification of fluorescence intensity changes on the plasma membrane for the mCherry channel in HeLa cells transfected with CFP or CFP-RhoC-V14. Error bar, ± SEM of 8 (with CFP) and 7 (with CFP-RhoC-V14) cells respectively. (E) FMNL2-GFP-myc wild type, S1072A, or S1072E were expressed in HEK293 cells and immunoprecipitated. Endogenous and ectopic FMNL2 were detected by FMNL2 antibodies. (F) Western blot of FMNL2 from HeLa lysates transfected with FMNL2 siRNA labeled with AlexaFluor 555 targeting 3'-UTR. (G) Representative images are shown at indicated time points for Figures 2F and S2H. Green: GFP; Red: AlexaFuor 555. Scale bars: 10 μm. (H) Quantification of fluorescence intensity changes on the plasma membrane for the GFP channel in HeLa cells transfected with FMNL2 siRNA labeled with AlexaFluor 555 targeting 3'-UTR which allowed FMNL2 wild type (FMNL2-GFP) or mutant (FMNL2-S1072E-GFP) DNA expression in the same cell. Error bar, ± SEM of 9 (FMNL2-S1072E-GFP) and 11 (FMNL2-GFP) cells respectively. Numbers indicate molecular weights (kD) in the Western blots. (A~C, & E~F).

Supplemental Figure S3

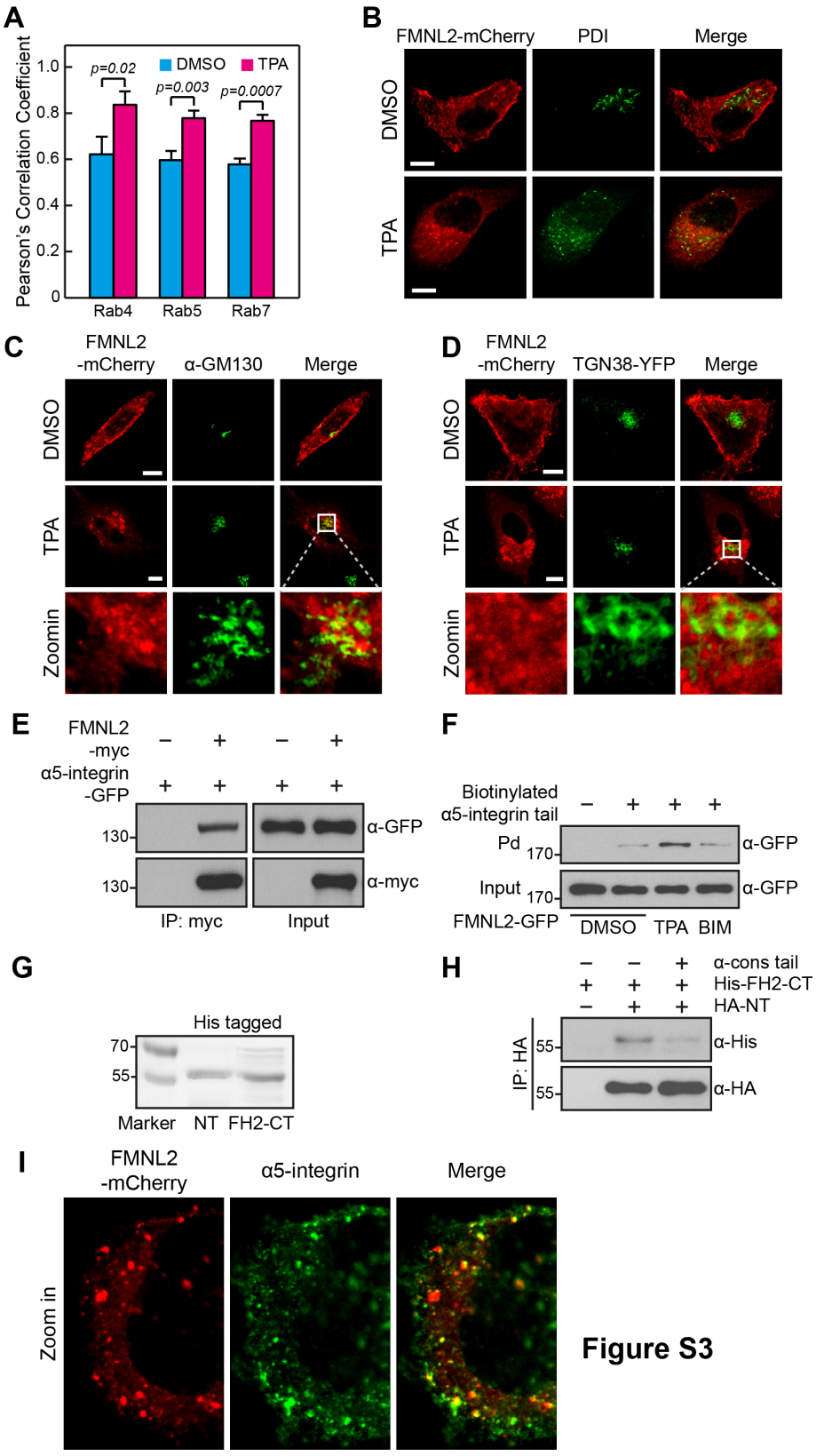

Figure S3

Figure S3. FMNL2 Colocalizes with Endosomal Markers and Interacts with α-integrins (Related to Figure 3)

(A) HeLa cells were transfected with FMNL2-mCherry and Rab proteins respectively. Cells were treated with DMSO or 200 nM TPA for 20 min at 37 °C. Pearson's correlation coefficient was used to quantify the colocalization of FMNL2 and Rab4, Rab5 or Rab7. Error bars: +SD, n=3, with 30 cells each time. P-values are indicated. (B) Representative images of FMNL2-mCherry and ER marker PDI (Protein disulfide isomerase) in HeLa cells with or without TPA treatment. (C) Representative images of FMNL2-mCherry and cis-Golgi marker GM130 in HeLa cells with or without TPA treatment. (D) Representative images of FMNL2-mCherry and trans-Golgi marker TGN38 in HeLa cells with or without TPA treatment. Scale bars: 10 μm. (E) Immunoprecipitation from HEK293 cells showing FMNL2 interacting with α5-integrin in cells. (F) Biotin-streptavidin pull down (Pd) of α5-integrin cytoplasmic tail from HEK293 cell extracts expressing FMNL2 constructs after DMSO, 20 nM TPA, 2 μM BIM treatment for 30 min. (G) Coomassie blue stained gels of the indicated purified proteins in Figure 3D. (H) Immunoprecipitation of purified HA-FMNL2-NT (15 μg) and His-FMNL2-FH2-CT (30 μg) with or without α-integrin conserved cytoplasmic tail (7 μg). (I) Enlarged images of different channels related to Figure 3G. Numbers indicate the molecular weights (kD) (F~H).

Supplemental Figure S4

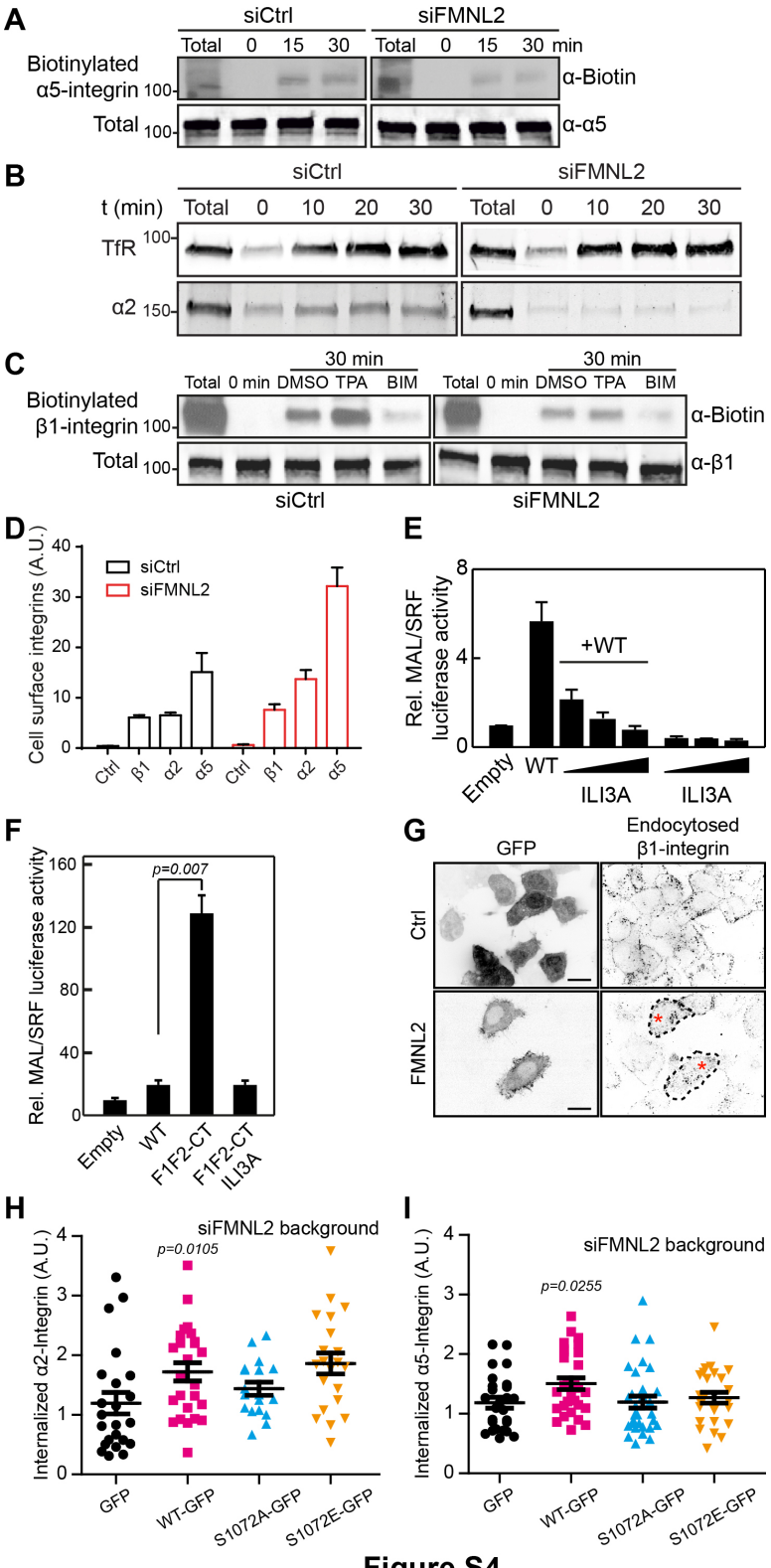

Figure S4

Figure S4. Characterization of FMNL2 Actin Assembly Mutant and Regulation of β1-integrin Internalization by FMNL2 (Related to Figure 4)

(A, B) Representative Western blots showing the immunoprecipitated total or endocytosed biotinylated α2- and α5-integrins or TfR under siCtrl or siFMNL2 conditions in HeLa cells. (C) Representative Western blots showing the immunoprecipitated total β1-integrin or endocytosed biotinylated β1-integrin in control or FMNL2 silenced HeLa cells treated with DMSO, 200 nM TPA or 2 μM BIM 30 min before endocytosis. (D) Cell surface levels of α2-, α5- and β1-integrins were measured in control or FMNL2 silenced HeLa cells. Error bars: + SEM (n=3). (E, F) HEK293 cells were transfected with FMNL2-GFP (WT), FMNL2-ILI3A-GFP, FMNL2-F1F2-CT-GFP, or FMNL2-F1F2-CT-ILI3A-GFP as indicated, together with MAL/SRF reporter 3DA.Luc and Renilla luciferase pRLTK. Black triangle indicates the increasing amount of DNA transfected. SRF activity was measured 24 h after transfection. Error bar: + SEM (n=3). P-value is indicated. (G) Representative images of image-based β1-integrin endocytosis assay. Confocal mid-sections of HeLa cells with transfected FMNL2-GFP in siFMNL2 background are shown here. Dashed lines indicate transfected cells. Red asterisk marks cells with increased β1-integrin endocytosis. Scale bars: 20 μm. (H, I) Quantified levels of endocytosed α2- and α5-integrins in HeLa cells expressing GFP, or GFP-tagged FMNL2 mutants under endogenous FMNL2 silenced background by imaging-based endocytosis assays. Graph shows mean line with error bar, ± SEM (n=3). Each point presents mean value of endocytosed integrin in one field of view. Indicated p-values are compared to the GFP control.

Supplemental Movie Legends

Movie S1. FMNL2 relocates upon PKCα activation (Related to Figure 2). Red: FMNL2-mCherry; Green: GFP-PKCα. Acquisition of images started when 200 nM TPA was applied to the cells. Images were acquired every 10 s. Scale bar: 10 μm.

Movie S2. FMNL2 relocation is inhibited when PKCα activity is inhibited by BIM-1 (Related to Figure 2). Red: FMNL2-mCherry; Green: GFP-PKCα. Cells were pre-treated with 2 μM BIM-1 for 30 min and then treated with 200 nM TPA. Acquisition of images started when TPA was applied to the cells. Images were acquired every 10 s. Scale bar: 10 μm.

Movie S3. The relocation of FMNL2 is reversible (Related to Figure 2). Red: FMNL2-mCherry; Green: GFP-PKCα. Acquisition of images started when 8 μM A23187 was applied to the cells. Images were acquired every 5 s. Scale bar: 10 μm.

Movie S4. FMNL2 relocates upon PKCα activation and localizes to α5-integrin positive vesicles (Related to Figure 3). Red: FMNL2-mCherry; Green: α5-integrin-GFP. Acquisition of images started when 200 nM TPA was applied to the cells. Images were acquired every 10 s. A small part of the upper movie is enlarged in the lower movie to show details of the co-trafficking of FMNL2 and α5-integrin. Scale bars: 10 μm.

Supplemental Experimental Procedures

Plasmids

Expression plasmids were generated and sequence-verified following standard cloning procedures. FLAG-FMNL2, FLAG-FMNL2-F1F2-CT, FLAG-mDia1 and HA-RhoCV14 were described previously (Kitzing et al., 2010; Vaillant et al., 2008). myc-FMNL2, FMNL2-myc, and myc-FMNL2-FH3 (aa 262-484) were sub-cloned into EFpLink with N-terminal or C-terminal myc-tag as indicated. GST-FMNL2-959-CT for protein purification was cloned into pGEX-6P-1 (GE Healthcare). HA-FMNL2-NT (aa 23-484) was cloned as GST-HA-FMNL2-NT into pGEX-6P-1, and the GST tag was cleaved during purification. His-FMNL2-NT was cloned into pET20 (Novagen) and His-FMNL2-FH2-CT was cloned into pET30 (Novagen). FMNL2 was cloned into pmCherryN1 (Clonetech), pEGFPN1 (Clonetech) or pWPXL vectors. Point mutants FMNL2-S1072A, S1072E and ILI3A (I704A, L1028A, and I1029A) were generated by site-directed point mutation. α5-integrin-GFP, GFP-PKCα and GFP-PKCα-T497A were described (Mostafavi-Pour et al., 2003). GFP-PKCα-CA was generated by deleting the first 30 amino acids (Soh and Weinstein, 2003) and subcloned into pEGFPC1 vector (Clonetech).

Cell Lines, Drug Treatments and Transfection

HEK293, HEK293T, HeLa and A375M2 (kind gift from Eric Sahai) cells were maintained in DMEM supplemented with 10% fetal bovine serum at 37°C in a 5% CO_2 environment. When needed, cells were treated with 5 nM to 200 nM TPA (Calbiochem), 2 μM BIM-1 (Calbiochem), 1 μM Gö6976 (Calbiochem) or 8 μM A23187 (Sigma). DNA plasmids were transfected with calcium phosphate methods for HEK293 and HEK293T cells, and with Fugene (Promega) for HeLa cells. siRNA (Qiagen) was transfected with HiperFect (Qiagen). A375M2 stable cell lines were generated by lentiviral transduction. Viruses were produced by transfecting HEK293T cells with packaging plasmid pSPAX2, envelope plasmid pMD2G and expressing plasmids pWPXL-GFP, -FMNL2-GFP, -FMNL2-S1072A-GFP, -FMNL2-S1072E-GFP,

or -FMNL2-ILI3A-GFP. Supernatants were harvested 48 h after transfection and A375M2 cells were infected. HeLa stable cell lines expressing shFMNL2 (V2LHS_384851, Open Biosystems) or shControl (a kind gift by Thorsten Stiewe) were generated similarly with lentiviral shRNAs.

Reagents and Antibodies

Cell culture reagents were purchased from PAA/GE Healthcare. Chemicals were from Sigma. α-phospho-(Ser) PKC substrate, α-PKCα, α-PKCδ, α-PKCε, α-PKCζ, α-biotin-HRP and α-tubulin were obtained from Cell Signaling Technology. α-PKCβ was from Santa Cruz. α-FMNL2 was purchased from Atlas Antibodies. α-α5 integrin (CD49e) was from AbD serotec. α-β1 integrin (CD29) antibody K20 was purchased from Beckman Coulter, 610468 was from BD Biosciences, 12G10 and EP1041Y were from Abcam. α-α2 integrin (MAB1998Z) was from Millipore. α-TfR (ab84036) was from Abcam. α-HRP-conjugated FLAG, myc and HA antibodies and HRP-conjugated secondary antibodies were from Sigma. Alexa Fluor conjugated secondary antibodies were from Invitrogen.

DNA Primers and siRNA Sequences

Point mutants FMNL2-S1072A, S1072E and ILI3A (I704A, L1028A, and I1029A) were generated by site-directed point mutation using the following primer pairs: 5'-AGGAGAGCCGTCAGGCGG-3' and 5'-CCTGACGGCTCTCCTCAC-3', 5'-AGGAGAGAGGTCAGGCGG-3' and 5'-CCTGACCTCTCTCCTCAC-3', 5'-CTTGCCGCCACTTTAAGG-3' and 5'-TAAAGTGGCGGCAAGATT-3', 5'-CAAGAGGCCGCAGCAGAATTA-3' and 5'-TTCTGCTGCGGCCTCTTGCTG-3', respectively. The actin assembly deficient mutant was generated according to (Heimsath and Higgs, 2012; Thompson et al., 2013). siRNA targeting sequences were: 5'-CACCATGGCTGCAATCCGAAA-3' (human RhoC), 5'-CTGCGGGCACATTCCCATAAA-3' (Hs_FMNL2_9, targeting 3'-UTR of human FMNL2, 3'-AlexaFluor 555 modified when indicated), 5'-AACCATCCGCTCCACACTAAA-3' (human PKCα),

5’-CCGGATGAAACTGACCGATTT-3’ (human PKCβI and PKCβII), 5’-AACTCTACCGTGCCACGTTTT-3’ (human PKCδ), 5’-CCCGACCATGGTAGTGTTCAA-3’ (human PKCε), and 5’-CGGAAGCATGACAGCATTAAA-3’ (human PKCζ).

Screening for the Effects of Formins on β1-integrin Endocytosis by Cell Spot Microarray

Cell Spot Microarrays (CSMA) were conducted as previously described (Rantala et al., 2011). Formin targeting siRNAs Hs_C14orf173_2 and 5 (INF2), Hs_DAAM1_6 and 7, Hs_DAAM2_7 and 8, Hs_DIAPH1_2 and 4, Hs_DIAPH2_1 and 4, Hs_DIAPH3_8 and 9, Hs_FHOD1_6 and 7, Hs_FHOD3_6 and 7, Hs_FMN1_7 and 8, Hs_FMN2_11 and 12, Hs_FMNL1_8 and 9, Hs_FMNL2_8 and 9, Hs_FMNL3_6 and 7, Hs_GRID2IP_5 and 6 (Delphilin), and control siRNA were purchased from Qiagen. Before plating HeLa cells on CSMA, the arrays where blocked with Lutrol F108 (Univar AB) for 15 min at room temperature. Cells were washed and harvested using HyQTase, then plated on CSMA. Endocytosis was measured 72 h after the reverse siRNA transfection. Antibody based integrin β1 endocytosis assay was carried out as described(Arjonen et al., 2012). In short, non-functional blocking β1-integrin antibody (K20) was labeled using AlexaFluor 488 protein labelling kit (Invitrogen). Cell surface β1-integrins of the CSMA with live cells were labeled with K20-AlexaFluor 488 for 1 h on ice. CSMA was then washed and the labeled β1-integrin was allowed to be endocytosed for 30 min at 37°C. The residual cell surface fluorescence was quenched using anti-AlexaFluor 488 antibody (Invitrogen) for 1 h on ice and fixed using 4% paraformaldehyde. Cells were then permeabilized and incubated with anti-mouse AlexaFluor 555 secondary antibody to label both internal and cell surface K20 pools (total β1-integrin). Endocytosed β1-integrin was normalized against the total β1 integrin. Nuclei were labeled using Syto60 (Invitrogen). Fluorescence intensities were measured using Laser microarray scanner (Tecan LS400) and ArrayPro Analyzer v4.5 software.

Protein Purification

The expression plasmid was transformed into E. coli BL21 (DE3). Bacteria were cultured in LB medium at 37°C until OD = 0.6 and induced with 200 μM IPTG at 22°C for 16 h or 12.5 g/L lactose at 30°C for 16 h. GST fusion protein was purified using Glutathione Sepharose 4B beads (GE Healthcare) as described before (Brandt et al., 2009). Proteins were dialyzed in 20 mM Hepes (pH 7.4), 25 mM $MgCl_2$, 5 mM EDTA and 5 mM DTT. The GST tag was cleaved during dialysis using Precision Protease (GE Healthcare) when necessary and the cleaved protein was recycled by running through the Glutathione Sepharose 4B once more. 6×His fusion protein was purified using Ni-NTA agarose beads (Qiagen) as shown before (Brandt et al., 2007).

In vitro Kinase Assay

Purified recombinant GST fusion PKC protein isozymes were purchased from ProQinase GmbH. 20 ng of each PKC isozyme and 1 μg substrate protein were incubated in 50 mM Hepes (pH 7.4), 150 mM NaCl, 5 mM EDTA, 5 mM DTT, 25 mM $MgCl_2$, 0.02% Triton X-100, 1 mM ATP and 5 μCi ^{32}P-γ-ATP at 30°C for 15 min. 1 μM Staurosporine (Sigma) was used when indicated. Kinase reaction was stopped by adding the SDS sample buffer. After running SDS-PAGE and fixation of the gel, autoradiography was performed with different exposure times.

Internalization Assay

Integrin or transferrin receptor (TfR) internalization assays were performed as described (Pellinen et al., 2008). 24 h after seeding, cell surfaces were labeled for 30 min with 0.5 mg/mL EZ-Link Sulfo-NHS-SS-Biotin (Pierce Chemical). Internalization was followed for the indicated times. The residual biotin was then removed from the cell surface by MesNa reduction (60 mM, 30 min), followed by iodoacetamide quenching (100 mM, 15 min). Total proteins were immunoprecipitated using the integrin or TfR antibodies. Internalized proteins were detected using Western blot with the HRP-linked biotin antibody. Total proteins were detected by integrin or TfR antibodies. Student's T-test was used to calculate the p-values.

Immunoprecipitation and Biotin-Streptavidin Pull-down

Cells were harvested and lysed in lysis buffer containing 20 mM Tris-HCl (pH 7.4), 150 mM NaCl, 2 mM EDTA, 0.1% Triton X-100, 2.5 mM sodium pyrophosphate, 1 mM β-glycerophosphate, 1 mM sodium orthovanadate, and complete protease inhibitors (Roche). Supernatants were collected after centrifugation and incubated with FLAG/myc/HA-conjugated agarose beads (Sigma) or Protein A/G beads (Santa Cruz) together with antibodies for 1 to 5 h at 4°C. For pull-downs, biotinylated α5/β1-integrin cytoplasmic tail peptides were pre-incubated with cell lysates respectively for 4 h (Pellinen et al., 2008). The peptide sequences were: α5-integrin cytoplasmic tail: Biotin-YKLGFFKRSLPYGTAMEKAQLKPPATSDA; β1-integrin cytoplasmic tail: Biotin-HDRREFAKFEKEKMNAKWDTGENPIYKSAVTTVVNPKYEGK; α-integrin conserved cytoplasmic tail: Biotin-WKLGFFKRKYEKM. Following a 1 h incubation with Streptavidin sepharose beads (GE Healthcare), samples were washed. Western blotting were performed as described previously (Brandt et al., 2009).

Membrane Flotation Assay

Membrane flotation assays were performed as described (Pan et al., 2012). Cells were lysed in cold TNE buffer (50 mM Tris-HCl pH 7.4, 150 mM NaCl, 5 mM EDTA, protease inhibitors and phosphatase inhibitors) and passed through 25G syringe 20 times. After centrifugation, supernatants were mixed with 67% Optiprep (Invitrogen) and loaded to SW60 centrifuge tubes. Each sample was overlaid with 2.5 mL 28% Optiprep and 600 μL TNE buffer. Ultracentrifugation was performed with SW60 rotor at 35,000 rpm for 3 h at 4°C (Beckman Coulter). 500 μL fractions were collected with the 2nd and 8th as the membrane and soluble fractions respectively.

Imaging-based Integrin Endocytosis Assay

HeLa cells were transfected with Qiagen Hs_FMNL2_9 siRNA (targeting 3'UTR) and EGFP or different FMNL2-GFP plasmids. Endocytosis was carried out as described with modifications (Gu et al., 2011). Cell surface β1-integrins were stained with primary and secondary antibodies for 1 h on ice and cells were allowed to endocytose the labeled

β1-integrins 30 min at 37°C. Cells were acid stripped on ice with stripping buffer, pH-restored with culture media and fixed. 3D confocal image stacks of fixed cells were acquired using Zeiss Axiovert 200M, Yokogawa CSU22 spinning disc microscope and 63X/1.4 oil objective. Images were analyzed using ImageJ. GFP positive cells were outlined by threshold-mask and the intensity of endocytosed β1-integrin was thresholded, background subtracted and quantified using ImageJ Analyse Particles and Integrated Density command. GraphPad Prism and Mann-Whitney test was used to calculate p-values for the endocytosis under different conditions.

Inverted Transwell Invasion Assay and Image Analysis

Invasion assays were performed as described (Kitzing et al., 2010). Cells were transfected with siRNAs 48 h before analysis. Cells were invading for 48 h before fixation, permeabilization and subsequent staining with DAPI and rhodamine phalloidin (Invitrogen). Confocal z-stacks of 100 μm were acquired for five random imaging fields of each insert with LSM 700 confocal microscope (Zeiss), using the 20X/0.75 objective. Quantification of the invaded and non-invaded cell number was done using the ImageJ Analyze Particle function. Student's T-test was used to calculate the p-values.

Expression of Cell Surface Integrins

HeLa cells were silenced 72h. Cells were harvested using HyQTase (Fisher Scientific) spinned down, lifted on ice and washed with ice-cold PBS. Cells were blocked using 2% BSA in PBS for 30min at 4°C and stained against α2, α5 and β1-integrins. Cells were washed in PBS and counterstained using Alexa-647 secondary antibodies for 30min at 4°C. Cells were washed in PBS and analysed with Accuri FACS.

MAL/SRF Luciferase Assay

MAL/SRF luciferase assay was performed as described (Baarlink et al., 2013). HEK293 cells were transfected with genes of interests, p3DA.luc and pRLTK reporter plasmids. 24 h after transfection, cell media were removed and cells were washed once with PBS. 200 μL 1× Passive lysis buffer (Promega) was added per 6-well. Cells were lysed on ice

for 20 min, scraped and centrifuged at 13,000 rpm for 15 min at 4°C. From 5 to 20 μL cell lysates were used for each assay. Firefly and Renilla luciferase signals were recorded sequentially by Luminoscan Ascent Microplate Luminometer (Thermo Scientific) using the Ascent software (Thermo Scientific) with 900 ms integration time. Firefly signal was normalized to Renilla signal for each sample.

Supplemental References

Arjonen, A., Alanko, J., Veltel, S., and Ivaska, J. (2012). Distinct recycling of active and inactive β1 integrins. Traffic *13*, 610–625.

Baarlink, C., Wang, H., and Grosse, R. (2013). Nuclear actin network assembly by formins regulates the SRF coactivator MAL. Science *340*, 864–867.

Brandt, D.T., Marion, S., Griffiths, G., Watanabe, T., Kaibuchi, K., and Grosse, R. (2007). Dia1 and IQGAP1 interact in cell migration and phagocytic cup formation. J. Cell Biol. *178*, 193–200.

Brandt, D.T., Baarlink, C., Kitzing, T.M., Kremmer, E., Ivaska, J., Nollau, P., and Grosse, R. (2009). SCAI acts as a suppressor of cancer cell invasion through the transcriptional control of β1-integrin. Nat. Cell Biol. *11*, 557–568.

Gu, Z., Noss, E.H., Hsu, V.W., and Brenner, M.B. (2011). Integrins traffic rapidly via circular dorsal ruffles and macropinocytosis during stimulated cell migration. J. Cell Biol. *193*, 61–70.

Heimsath, E.G., and Higgs, H.N. (2012). The C terminus of formin FMNL3 accelerates actin polymerization and contains a WH2 domain-like sequence that binds both monomers and filament barbed ends. J. Biol. Chem. *287*, 3087–3098.

Kitzing, T.M., Wang, Y., Pertz, O., Copeland, J.W., and Grosse, R. (2010). Formin-like 2 drives amoeboid invasive cell motility downstream of RhoC. Oncogene *29*, 2441–2448.

Mostafavi-Pour, Z., Askari, J.A., Parkinson, S.J., Parker, P.J., Ng, T.T.C., and Humphries, M.J. (2003). Integrin-specific signaling pathways controlling focal adhesion formation and cell migration. J. Cell Biol. *161*, 155–167.

Pellinen, T., Tuomi, S., Arjonen, A., Wolf, M., Edgren, H., Meyer, H., Grosse, R., Kitzing, T., Rantala, J.K., Kallioniemi, O., et al. (2008). Integrin trafficking regulated by Rab21 is necessary for cytokinesis. Dev. Cell *15*, 371–385.

Rantala, J.K., Mäkelä, R., Aaltola, A.-R., Laasola, P., Mpindi, J.-P., Nees, M., Saviranta, P., and Kallioniemi, O. (2011). A cell spot microarray method for production of high density siRNA transfection microarrays. BMC Genomics *12*, 162.

Soh, J.-W., and Weinstein, I.B. (2003). Roles of specific isoforms of protein kinase C in the transcriptional control of cyclin D1 and related genes. J. Biol. Chem. *278*, 34709 – 34716.

Thompson, M.E., Heimsath, E.G., Gauvin, T.J., Higgs, H.N., and Kull, F.J. (2013). FMNL3 FH2–actin structure gives insight into formin-mediated actin nucleation and elongation. Nat. Struct. Mol. Biol. *20*, 111–118.

Vaillant, D.C., Copeland, S.J., Davis, C., Thurston, S.F., Abdennur, N., and Copeland, J.W. (2008). Interaction of the N- and C-terminal autoregulatory domains of FRL2 does not inhibit FRL2 activity. J. Biol. Chem. *283*, 33750 –33762.